Robust genetic algorithm for high-accuracy particle position estimation in three-dimensional particle image velocimetry applications

P. Padilla Sosa
J. E. Valdez
L. R. Berriel
National Institute of Astrophysics, Optics and Electronics
Tonantzintla, Puebla
México
E-mail: padilla@inaoep.mx

L. R. Sahagún Ortiz
Universidad de Guadalajara
Guadalajara, Jalisco
México

M. Funes-Gallanzi
AVNTK S.C.
Guadalajara, Jalisco
México

Abstract. A method for three-dimensional particle position estimation employed in particle image velocimetry applications is presented. The method includes the application of a robust optimization process, which involves the use of a genetic algorithm. The algorithm derives particle position by pattern matching theoretical to experimental images, using the concept of image peak signal-to-noise ratio as the objective error measure for this comparison. To produce sufficiently accurate theoretical images comparable to experimental images for positioning purposes, it is found that a Lorenz-Mie treatment of the seeding scattering field was required, which also took into consideration the incident wavefront. The use of a genetic algorithm for positioning proved to be more accurate and faster than a Nelder-Mead algorithm combined with neural nets used previously. This method has also been shown to be an effective means of isolating contaminant particles in velocimetry images, which can substantially increase the overall error. We discuss some aspects of the theory regarding this method, illustrate the ideas with a simple experimental image, as well as detail our implementation of a pattern-matching approach combined with a genetic algorithm for positioning purposes.
 [DOI: 10.1117/1.1533038]

Subject terms: diffraction pattern; genetic algorithms; particle position estimation; tunneling velocimetry; particle image velocimetry.

Paper 020146 received Apr. 17, 2002; revised manuscript received July 25, 2002; accepted for publication July 31, 2002.

1 Introduction

In recent years, emphasis has been placed on obtaining the third velocity component, normal to the illuminated plane in particle image velocimetry (PIV), as it is important to obtain 3-D velocity measurements. There are different and numerous optical arrangements that have been proposed for providing instantaneous information in PIV to obtain three-dimensional position information.[1]

Velocimetry particle images show a scattering field that is dependent on their relative 3-D position when illuminated in a volume, such as when they are holographically recorded or imaged using tunneling velocimetry.[2]

The application of holography to PIV is almost as old as its application to particle sizing. Originally, the technique was named holographic velocimetry (HV) and made use of the in-line arrangement. Since then substantial progress has been made but not enough for its industrial use. The availability of commercial PIV systems has brought holography back to researchers' attention, as it appears to be a natural successor to standard PIV, and in the process has been renamed HPIV. However, there is a difference between HV and HPIV: HV refers to full 3-D experiments, whereas HPIV simply means the holographic recording of PIV images. More specifically, in HPIV a light sheet is used to illuminate the particles and the result is just a 2-D velocity map with two or three components. Thus, most analysis methods and software used in PIV also work with HPIV. This is far from being the case with HV, in which the third dimension substantially increases the complexity of the data, analysis methods, and software required.

The tunneling velocimetry technique involves in-line illumination of a volume of interest, achieved through a single instrument using a single optical access point, thus obtaining seeding particle scattering images produced within said volume. Figure 1 shows an image taken by this method. These images have to be interpreted to obtain 3-D information of the particle position. The diffraction field can be deduced from a single CCD camera position for a range of x-y-z particle positions, opening the way for using a single camera in practical experiments. This previous point is important in cases where there is restricted optical access to flows of interest, such as those found in turbomachinery, where only one camera is often what can be accommodated. Therefore, it is of crucial importance to develop a processing technique capable of taking sufficiently accurate 3-D velocity measurements from a single CCD image.

Recently, a lot of research has been focused on the analysis of particle image fields when illuminated by arbitrary incident beams, as opposed to the plane wave assumption of the classical Lorenz-Mie theory.[3] This treatment is known as generalized Lorenz-Mie theory (GLMT). To produce theoretical images of a quality quantitatively comparable to experimental images, it was found that a general-

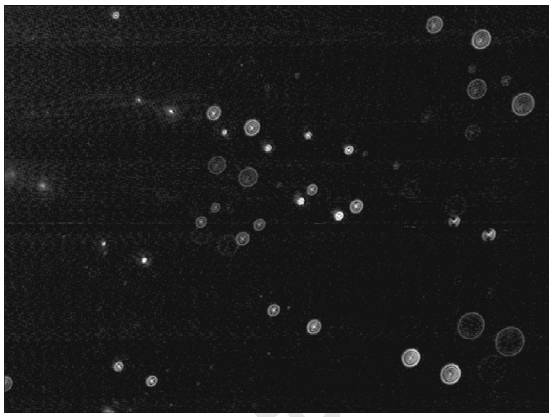

Fig. 1 Sample double-pulsed 6.5-μm polystyrene particle images at a magnification of 1.2× using the tunneling velocimetry technique.

ized Lorenz-Mie treatment of the scattering field was required, which also considered the characteristics of the incident wavefront. A program for calculating the GLMT scattering field of particles at any given position when illuminated by plane, Guassian, spherical, or elliptically shaped incident beams has been previously reported by our group for particle image velocimetry applications.[4] However, a detailed model of the behavior of illuminated particles is insufficient to produce a practical positioning algorithm, unless means are found to make it applicable for low-magnification conditions, so that correspondingly large investigation volumes can be achieved.

A particle-positioning method using GLMT to create theoretical seeding particle images, and embedding the genetic algorithm search concept, was devised and is described in the present work. The use of a genetic algorithm overcomes the limitations of using a treatment combining GLMT, a Nelder-Meade simplex algorithm,[2] and a neural net approach as previously reported.[5] The Nelder-Meade algorithm is one of the most widely used direct search methods for nonlinear unconstrained optimization, though the theoretical underpinnings of the algorithm, such as its convergence properties, are less than satisfactory. These limitations primarily involve low computational efficiency and the need to retrain a net for each set of experimental conditions.

Moreover, the related problem of searching for the best particle pairing, from which velocity is derived in particle tracking algorithms, is a lengthy process in the presence of a large number of particles. However, genetic algorithms are a promising practical alternative to use for particle positioning purposes. Sheng and Meng,[6] who explored a velocity extraction technique based on a genetic algorithm for application in 3-D holographic particle images, showed that the method was more accurate in velocimetry measurements with low seeding density regions and large velocity gradients. One important point of this method is that we can increase the speed of the particle-pairing search by using several mutation and cross-over operations and some *a priori* knowledge at the initialization stage.

2 Brief Remark

In the initial work on 3-D particle positioning,[5] a simplified model was used to represent the scattered field of a particle in a laser beam. This simplified model was employed to develop an understanding of the requirements for a high-accuracy robust 3-D positioning algorithm because of its computational simplicity. We considerd the case of a particle-scattered field modeled by Fraunhöfer diffraction, digitized with varying dynamic range in the spatial and intensity domain and with *a priori* knowledge of the particle diameter estimate, and an initial position estimate. We primarily considered digitization issues and provided a means to position particles in 3-D.

By the process of digitizing at low magnification, we cease to have a recognizable digital representation of the diffraction pattern. However, it is assumed that it is still unique. This issue of uniqueness, i.e., that given estimate and objective images there should be one and only one position capable of minimizing an error function, depends on the error being independent for each axis and needs to be corroborated. A particle image, known as the objective image, with a center at (x,y) and a distance z from the focal plane was used as the reference. Another particle image, known as the estimated image, was generated with an incremental displacement along each axis in turn. Thus, if these two images are subtracted, the resulting error characteristics due to each class of incremental displacement can be ascertained. For example, a displacement between the estimated and objective image in the x direction results in an asymmetric error in the direction of said axis, while a displacement in z direction results in a concentric symmetric error distribution. In Fig. 2, we can see the differing characteristics of errors in the three principal axes. It was shown that a process of iteration can be implemented, where from an initial position estimate the algorithm could iterate until the difference between the digital representation, the objective, and the estimate image was minimized and that said minimum corresponded to a unique position.

One difficulty involved in implementing a pattern-matching approach to particle positioning is the ambiguity normally produced by a simplified treatment of differentiating particles in front of and behind the focus plane. Previous works employing a more detailed treatment[4,7] have shown that the scattered intensity field produced by micron-sized particles is not symmetric about the focus plane. Therefore, there can be no ambiguity of particle position for particles on either side of the focus plane. This fact can be seen clearly in Fig. 3, which shows a plot of particle intensity distribution in a range of -5 to $+5$ mm about the focal plane for a 21-μm glass particle using the generalized Lorenz-Mie theory.

A simplified algorithm that used a Nelder-Mead nonlinear search strategy to estimate particle position was initially implemented. To achieve an initial estimate of the z coordinate, a conventional neural net was constructed, broadly similar to one described previously,[8] while a centroid estimate was employed to yield a first estimate of in-plane position. The overall light intensity estimate can be obtained by calibration, and so this was taken as a known subject to an experimental error. The five parameters optimized were: the three coordinates of x position, y position, z position, the particle diameter, and the peak intensity. The peak intensity was included because even though cameras may be calibrated knowing the prevailing light conditions, these cannot be accurately estimated given digital technolo-

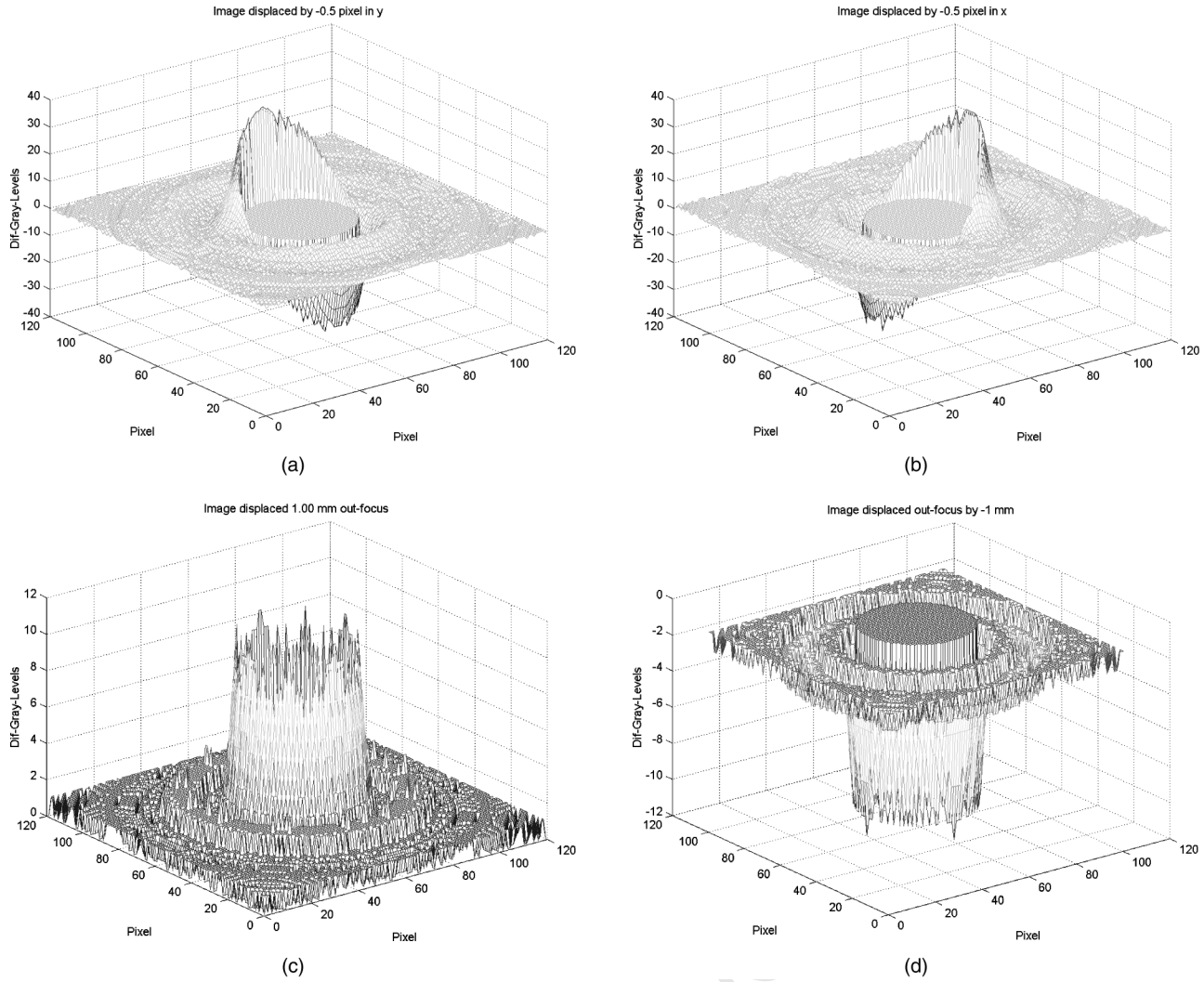

Fig. 2 Mesh plots show the effect of an error in the *x,y,z* component: (a) and (b) are asymmetric large errors in the direction of the axis, and (c) and (d) show a concentric symmetric error in the *z* component.

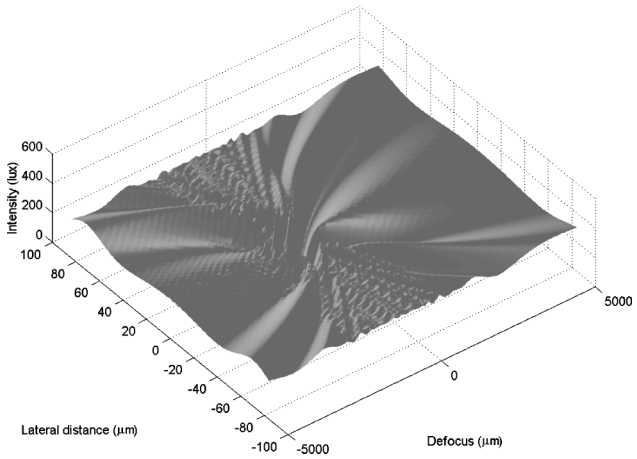

Fig. 3 Calculated particle intensity field for a 21-μm glass particle over a 1-cm depth of defocus using the generalized Lorent-Mie theory (GLMT).

gy's sensitivity to such factors as temperature and power source variations.

2.1 *Basic Problem*

Although the initial work proved successful in understanding the needs and limitations involved in constructing an algorithm for 3-D particle positioning, it proved inadequate in a number of respects.

1. Experimental data requires a detailed model for accurate positioning that is quite complex. When typical noise is added, such as noise in CCD images, it results in a number of local minimum points of the error objective function. Gradient methods in this case of multiple minima find it difficult to resolve and find the global minimum, corresponding to the actual particle position. In the previous work we used a Nelder-Mead algorithm. This kind of optimization method is efficient when the function has a few local minima value reasonably close to the initial conditions. However, in the general case, one requires

working with a very complex problem with multiple minima value in large volumes. So a method of global optimization is required, able to deal with this type of surface.

2. When applying the GLMT code to model the objective image and compare to the experimental image, the algorithm slowed down to an unacceptable rate as it was fully implemented in MATLAB. This is an interpreted language, rather than having the more computationally intensive sections programmed and compiled in C++ for speed. So it was necessary to make a conversion of some subroutines from MATLAB to C++, though this is still in progress and will be reported elsewhere.
3. The use of neural nets involved the extra step of net training, configuration changes for each set of conditions, and a complex overall system.
4. The merit function used to obtain the *x*, *y*, and *z* positioning between images was median absolute error in intensity. However, this arrangement proved to be inadequate. So, the merit function was changed by peak signal to noise ratio (PSNR).[9] There are many versions of signal to noise ratios, but PSNR gives better sounding numbers than other measures in the sense that it yields a low-magnitude increasing positive number for lower errors, which is useful intuitively and as many optimization subroutines maximize by default.

Other aspects of this simplified treatment must be considered before going on to an experimental image analysis and are related to finding the center of the particle image. There is a preprocessing of the image that consists in image enhancement. The first step consists of finding an optimal threshold for the image. The values of pixels below this threshold level were set to zero and the rest were set to one. The image was thus converted to a binary image. The binary image was then processed by a dilatation morphological operation, with a circular structuring element. A binary dilation of an object has the effect of increasing its geometrical area. The aim of this process was to obtain well-defined circular particle images and to achieve a center estimate of the resulting particle footprint as a first estimate of the particle position in *x* and *y*. On the other hand, a neural net was then applied to find an initial estimate of the *z* position. An initial estimate of particle diameter and peak intensity was obtained by microscope measurement and camera calibration, respectively.

As far as the accuracy of the *x*, *y*, and *z* estimates are concerned, numerical simulations were carried out. These simulations assumed that *x* and *y* coordinates have an error of no more than 0.5 pixels initially (the accuracy of the first pass of the algorithm using a centroid estimation) and that the *z* coordinate could be estimated by application of the neural net module to within 1 mm initially.

If the initial position estimate for *z* were chosen at random, eliminating the neural net module, the algorithm would in general not converge by using a Nelder-Mead routine because of the multimodal nature of the problem as discussed previously. The noise assumed for this work was a variation due to shot noise of 1 gray level for the Fraunhöfer image with a background noise of 20 gray levels. These two parameters were taken as typical of the sort of CCD camera used after being adapted for low-light applications, both being independent of the data.

In the next section we propose a refinement of the method previously used, to make high accuracy particle velocimetry measurements, and achieve a robust algorithm exploiting the scattered energy field, through using pattern matching and genetic algorithms.

3 3-D Genetic Positioning Algorithm

3.1 *Introduction to Genetic Algorithm*

There are two main strategies of searching to resolve the optimization problem. One of them is based on genetic algorithms (GA). This is a method using a global search strategy, while the alternative corresponds to implementing a local search strategy based on gradients, continuity, etc. Furthermore, other techniques have been implemented such as a hybrid method[10] to produce fast global optimization.

The fundamental idea of genetic algorithms is based in the rules of natural selection. There are three basic concepts relating to this algorithm: reproduction, gene cross-over, and mutation. Organisms can pass beneficial and survival-enhancing traits to new generations. In this approach, the variables are represented as genes on a chromosome. The population on which the GA evolution takes place comprises a group of chromosomes that represent possible solutions of the problem, and from which parents for a new generation are selected. By evaluating fitness values for all chromosomes, a particular group of chromosomes is selected from the population as parents to generate offspring (a new generation of the problem). The better the fitness, the greater the chance a chromosome stands of being selected as a parent for reproduction. Fitness values for offspring are evaluated in the same fashion as their parents, and then chromosomes in the current population are replaced by offspring based on certain replacement strategies. Such a GA cycle is repeated until the termination criterion is reached. A more complete discussion of genetic algorithms can be found elsewhere.[11,12]

For this application, an existing genetic algorithm optimization toolbox was used[13] to implement a global search strategy to estimate velocimetry seeding particle positions in three dimensions. This toolbox contains a portable algorithm in a mathematical environment with capabilities that have been tested with different nonlinear, nonconvex, multimodal functions, such as the Fraunhöfer formalism.[14] Results have shown that the software is capable of finding adequate solutions at a lower computational cost than simulated annealing and other conventional algorithms that are applicable to convex regular functions, such as the Nelder-Mead method and adaptive random search.

A proper selection of genetic operations and their impact on the evolution process is critical to a successful GA implementation. Thus, the general method and particular set of genetic operators implemented for this problem is described next.

3.2 *Encoding Scheme*

Typically, a particle image with a known position $c_0 = (x_0, y_0, z_0)$ was generated and modeled by a Fraunhöfer approximation, with the particle being known as the objec-

Table 1 Comparison of the rms out-of-focus positioning errors for the two algorithms. The simulated particle was moved out of focus by a random displacement of 1 mm (in a light sheet) and 10 mm (in a volume) away. The table shows the errors normalized to the depth of focus for 2× magnification.

	Fraunhöfer Approx. rms out-of-focus error in a light sheet		Fraunhöfer Approx. rms out-of-focus error in a volume		GLMT	
	Error	Run time (min)	Error	Run time (min)	Error (mean vel.)	Run time (hours)
Nelder-Mead algorithm	12	17	105	18	+2.8%	3.1
Genetic algorithm	1	3	4	3	+2.3%	2.5

tive image I_o. A second particle image I_e was then generated with initial conditions $c_1=(x_1,y_1,z_1)$ as previously described, except for the z estimate, which was initialized as a random position both within a light sheet and within a volume to explore a method not using neural nets. We apply a genetic algorithm to find the best pairing for each particle. So, both images were then matched according to the following fitness criterion to quantify their similarity:

$$\text{fitness}=20^{*}\log_{10}\left\{\frac{1}{\text{sqrt}[\text{mean}(I_o-I_e)^2]}\right\}.$$

Therefore, the position of the estimate image can be varied to maximize the similarity of both images, which is a typical optimization problem. Such a problem is capable of being cast as an evolutionary problem by coding an estimated particle position as a chromosome-evolving subject to a fitness criterion provided by the PSNR metric when matching images. Once the GA algorithm produces the optimum chromosome (i.e., the estimated particle position), the error between the estimated position and the known objective particle position can be calculated and can form the basis for the results discussed.

3.2.1 *Initial population*

The initialization step creates the first generation of chromosomes for evolution, and these are normally randomly and uniformly distributed in the solution space for fast convergence. Here the initial population was randomly generated and contained 120 individuals.

3.2.2 *Selection function*

The function that selects individuals to produce generations is devised as follows. A probabilistic selection is performed based on the individual's fitness with the better individual in the population.

There were several selected functions, but a ranking selection function method is used and based on the normalized geometric distribution with a probability $p_g=0.08$.

3.2.3 *Operator*

During the search stage, genetic operators need to be defined, and their overall effect on the system evolution also has to be quantified. The two fundamental types of operators are cross-over and mutation. These operators were used to create new solutions based on existing solutions in the population using a floating-point representation.

For instance, cross-over operators take two individuals and produce two new individuals. In the case of simple cross-over, a random number s is generated from a uniform distribution from 1 to m (where m is the total length number of bits in a chromosome) and creates two new individuals. Other operators can be used, such as arithmetic and heuristic operators.

Mutation alters one or more genes (position in a chromosome) with a specific probability. Mutation is employed to give new information to the population and also prevents the population from becoming saturated with similar chromosomes. Nonuniform mutation, uniform mutation, multinonuniform mutation, and boundary mutation have all been implemented in the approach used for this method. For the optimization of the estimation Fraunhöfer function, a float genetic algorithm was employed with the previously mentioned operators.

3.2.4 *Termination function*

The GA algorithm moves from generation to generation selecting and reproducing parents until a termination criterion is met. For this application, the criterion used was a specified maximum number of generation (80), an achievement of a user-defined optimal value for the error (27 dB), or a variation in the error function from generation to generation of less than $\varepsilon=10e^{-4}$.

4 Simulated Results

A robust method using pattern matching and a genetic algorithm to find the optimum particle position in three dimensions that maximized the peak signal-to-noise ratio was implemented and tested on both simulated and experimental data. To better understand the performance of this approach, it was compared to the performance of a previously used Nelder-Mead strategy. This new approach was found to perform faster, with a higher accuracy, and without the need to obtain an initial z position estimate, thus reducing the computational cost and making the method simpler.

Table 1 shows an error comparison between a Nelder-Mead algorithm and a genetic algorithm for a 15-run test study. Both algorithms were tested on a Pentium IV running at 1.2 GHz. The more demanding GLMT calculations were performed on a 2.2 GHz machine. The genetic algorithm provided both a faster processing speed and lower error than a Nelder-Mead algorithm. Using a Nelder-Mead

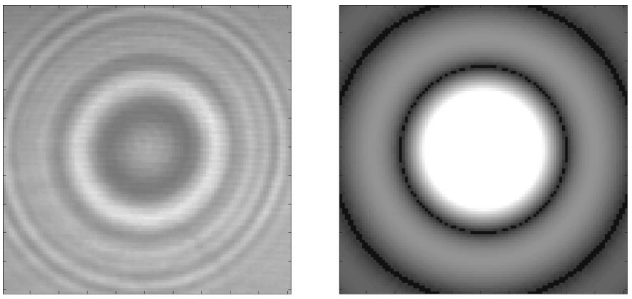

Fig. 4 Comparison of (a) experimental and (b) Fraunhöfer calculate representations of the particle scattering field.

algorithm in a volume, we have a factor of nine times higher error than in a light sheet. This is primarily due to the fact that in some cases, the algorithm converges to a local minimum, not a global minimum, thereby disproportionately increasing the resulting error. Even in the case of a light sheet, where both algorithms converge, the Nelder-Mead approach results in an error more than ten times higher than the GA algorithm proposed. Processing time for the GA algorithm is more than five times lower than that taken by a Nelder-Mead approach. Finally, the error produced by applying the proposed GA algorithm to a volume is only four times higher than that obtained in a light sheet, due to the rapid convergence of the algorithm to the general area of the global minimum. All simulation values shown in Table 1 have been normalized by the depth of focus available for the modeled conditions at a magnification of 2×, i.e., a depth of field of 44 μm. On the other hand, the right-hand side of this table shows experimental results expressed as a percentage of true velocity for both a GA and a Nelder-Mead approach, rather than as a positional error, as in the other two columns.

To study the relevance of the Fraunhöfer approximation on a real image, a typical forward scattering setup was used for experimental recording, and a particle scattering image was modeled using the Fraunhöfer approach. Although the comparison between the experimental image and the Fraunhöfer image is not very close, Figs. 4(a) and 4(b) illustrate why this approximation was used. The experimental and approximated image are qualitatively similar, and the approximated image is very easy to compute for testing purposes. The experimental image was an 18-μm-diam spherical particle that was illuminated by a laser wavelength of 638 nm in the forward mode, and viewed through a 90-mm focal length lens at a magnification of 7.8×.

The results for the position estimates were broadly similar for the x and y component, as can be expected. However, the result for the performance in the z component is worthy of note and is shown in Fig. 5, all normalized with respect to the depth of focus. Figure 5(a) shows the performance of the absolute error versus magnification for different width of sampling intervals in the image plane. As expected, higher spatial resolution and a corresponding larger number of sampling points per millimeter in the image plane (i.e., smaller sampling intervals resulting from smaller pixels results in more detailed information about the particle image in the object plane) leads to lower error (all calculations were made for 8-bit resolution). Figure 5(b) shows a complementary view of error versus magnification for a range of intensity resolutions, where spatial resolution was kept constant at 11 μm. Again, as expected, a larger intensity resolution results in lower error, but at a diminishing rate, so there is a large decrease in error in going from 8 to 10 bits, but a much more modest reduction from 10 to 12 bit. Therefore, a 10-bit camera with 11 μm of resolution pixel could be expected to achieve a positional error of 5 μm at a magnification of 7.8×. However, this error could be reduced by the use of a full GLMT treatment, where particle images vary much more significantly as a function of displacement in the z direction than a Fraunhöfer simplification, particularly in the focal plane region.

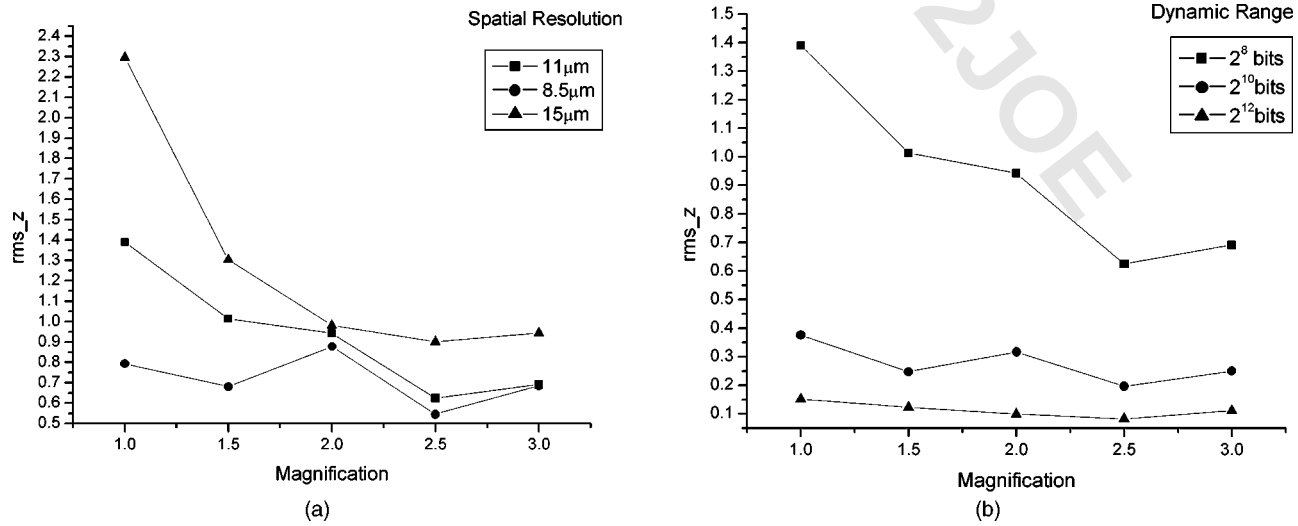

Fig. 5 Performance of the robust positioning method using a genetic algorithm: positional error versus magnification (normalized with depth of focus) for a range spatial resolution of pixels and a range intensity resolution of 8, 10, and 12 bits ADCs.

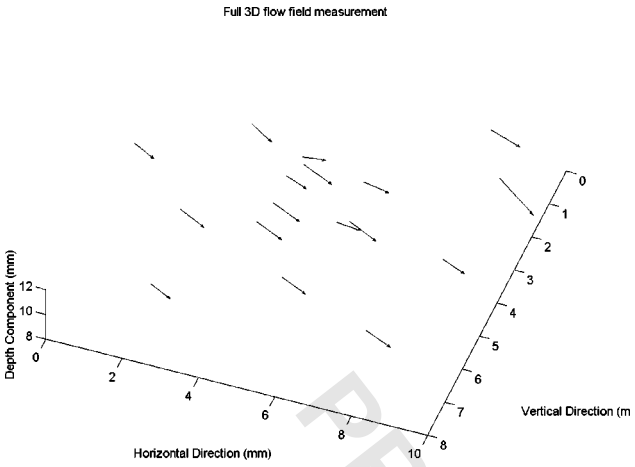

Fig. 6 Three-dimensional flow field analysis of data shown in Fig. 1.

5 Experimental Results

Once the method was tested with simulated data, an experimental image was investigated (see Fig. 1). For the experimental case, a full GLMT formulation of the scattering field was used rather than a simplified Fraunhöfer approximation. The error metric was used again to maximize the peak signal-to-noise ratio between the experimental and estimated images. We used manually assisted particle recognition just to identify and separate particles in the first and second pulses. Thus, the particle centroids were located, separated, and taken as initial centroids. The time taken to process this image was at first prohibitively high, due to the heavy computational requirements of GLMT. Therefore, the method was refined so that it kept previously computed data in a look-up table, which could be subsequently inspected before doing a GLMT calculation, thereby reducing significantly the time taken to process the experimental image.

The experimental image was obtained by backscattering tunneling velocimetry (TV), as described elsewhere,[2] though a holographic image can equally be used. The seeding material was polystyrene sized to 6.5 μm, injected through a nebulizer, flowing in a free jet at a speed of 9.5 m/s and an angle of 32 deg to the image plane. A frequency-doubled Nd/YAG laser with energy of 100 mJ/pulse and a pulse separation of 100 μs illuminated the seeding. The resulting image was recorded at a magnification of 1.74×, and viewed through a 90-mm SIGMA lens.

Figure 6 shows the resulting raw velocity field in 3-D. There are only a few particle pairs in this image, but it does serve to illustrate the feasibility of the method. However, there is one point that is apparent from a review of the velocity vectors and the corresponding experimental image. Namely, there are some vectors that have a large error. After further investigation, it was concluded that the jet contained some water particles that had not yet evaporated, as well as the intended polystyrene seeding, as the seeding was not heated as is normally done. Since the GLMT code requires knowledge of the complex refractive index and seeding particle size, it generated erroneous positions for those seeding particles that were not made from the same material as the seeding. Therefore, this is an effective means to isolate contaminant particles in velocimetry images. However, there are some cases such as when three-state anemometry is applied,[15] where a number of seeding populations are used and need to be identified separately. (Anemometry is a technique that seeks to derive fluid velocity, temperature, and density by the differing trajectories of a number of seeding populations specially selected for this purpose). For this type of application, where a mixture of seeding diameters are used, the algorithm needs to be further refined to identify position and population information. Our group is actively developing this last method. This is currently the subject of much research and beyond the scope of this article, so it will be reported separately in the near future.

The limitations applicable to this method relate primarily to the seeding density that such an approach is able to tackle. The technique is aimed at practical applications in hostile industrial environments, where seeding densities are typically quite low to medium at best and noise is high.

It is a small point but worthy of mention that although holography possesses the advantages of large sensing areas and high resolution, the sensing areas are limited by scattering energy levels required from seeding particles, while the benefits of high resolution are limited by background noise. Sensing areas can be increased by using, for example, a forward scattering arrangement, where particle scattering efficiency is larger, though such arrangements are much more complicated than conventional in-line methods and often also require multiple optical access, limiting the applicability of these approaches in industrial applications. Moreover, the latter advantage is applicable for the case where noise is low, rather than industrial applications where noise levels can be high. In general, there will be no change in precision as resolution is increased in the presence of noise, an intuitive result that has been supported by experimental evidence.[16]

In any case, high-density recording in holographic particle image velocimetry (HPIV) is difficult to achieve at an acceptable signal-to-noise ratio. Typically, at a density of 10 particles/mm^3, holographic particle image velocimetry encounters speckle noise.[17] Although speckle noise can be controlled to various extents at the cost of increased complexity, densities are still rather low, leading to measurement rates of the order of 0.5 measurements/mm^3 or less using correlation approaches. To overcome this problem, there has been some work on more advanced 3-D velocity extraction algorithms, which can cope with the low seeding densities of HPIV using genetic algorithms.[6] This particular method, however, still uses a low accuracy convoluted method to obtain the particle vectors in the first place. So, speckle noise limits the potential measurement density of HPIV in industrial applications, pointing to tracking methods as the most appropriate for 3-D velocity estimation, due to the low particle seeding density required by these methods compared to frequency approaches.

The particle tracking method, however, has been shown to work successfully in HPIV, also achieving a considerable reduction in data processing compared to frequency methods, as shown by our early work in this area.[18] This early work was followed up by further work in the field of interrogation of 3-D particle image fields.[19–21] However, this work now proposes, for the first time, using the particle scattering field directly in a 3-D particle-tracking mode

suitable for noisy hostile environments with limited optical access, as opposed to the previously used correlation-based or stereoscopic methods.

Clearly, in the case of HPIV images obtained in laboratory conditions, the seeding density can be quite high and unsuitable for an approach such as the one proposed here. In a high-density HPIV case, the overlap of particle scattering fields would lead to confusion, and therefore illustrates a limitation of the applicability of the method. Moreover, although the software developed to date is being speeded up by optimization/compiling/introduction of look-up tables for reusing computationally intensive data, the computational requirements involved in high-density image analysis would be prohibitive, thus representing a further limitation to the applicability of this method for high density velocimetry images.

6 Conclusions

A robust three-dimensional positioning algorithm for low and medium density particles was successfully implemented, which is based on pattern matching a calculated particle image using GLMT an experimental images. This method employs a genetic algorithm for finding the optimum position estimate with a peak signal-noise ratio criterion for estimating error. The mean measured velocity of this method and particularity for this test problem was estimated to be of the order of 9.78 m/s, some 3% higher than the actual velocity, neglecting pairing particle errors that would normally arise in conventional images. This method allows a reduction of magnification down near unity at an accuracy in the region of 20 μm, when used together with a GLMT treatment of particle diffraction.

The method requires an amount of data to be analyzed that is much lower than for other methods (ring-counting intensity estimation or other commonly used methods), and we employed lower magnifications than these methods, which effectively enlarges the feasible investigation region.[8,22,23] Moreover, the method demonstrated a capability to identify contaminant seeding particles, which typically do not satisfy flow-following criteria and therefore increase error.

Current work is oriented toward implementing a GA particle-pairing strategy using a continuity criterion for the objective function. Much work remains in refining codes, such as speeding it up, including all forms of lens aberration, and extending it to simultaneously positioning and identifying seeding population to which a given seeding image belongs. Nevertheless, the method described is able to position seeding velocimetry particles in 3-D based on a particle scattering field, even using HV data, using a single image and at low magnification, automatically and with high accuracy.

Acknowledgments

The Mexican National Council for Science and Technology (CONACYT) supported this work through project No. 35062-E, which is greatly appreciated. P. Padilla and J. E. Valdez also give special thanks to CONACYT for granting research scholarships. A special thanks to Dr. D. Moreno and Dr. J. A. Guerrero for their collaboration with this work.

References

1. D. H. Klaus, ''Three-dimensional particle velocimetry,'' *Meas. Sci. Technol.* **6**, 742–753 (1995).
2. M. Funes, ''Tunnelling velocimetry: consilience comes to the study of fluid dynamics,'' *10th Int. Symp. Appl. Laser Techniques Fluid Mechanics*, Instituto Superior Tecnico, LADOAN, Lisbon, July 10–13, 2000.
3. G. Gousbet and G. Gréhan, ''Sur la généralisation de la théorie de Lorenz-Mie,'' *J. Opt.* **13**, 97–103 (1982).
4. D. Moreno, F. Mendoza, and M. Funes-Gallanzi, ''Particle positioning from a single CCD image: theory and comparison to experiment,'' *Appl. Opt.* **39**(28), 5117–5124 (2000).
5. P. Padilla and M. Funes-Gallanzi, ''Low-magnification particle/ Positioning for 3D velocimetry applications,'' *Opt. Laser Technol.* **34**, 59–68 (2002).
6. J. Sheng and H. Meng, ''A genetic algorithm particle pairing technique for 3D velocity field extraction in holographic particle image velocimetry,'' *Exp. Fluids* **25**, 461–473 (1998).
7. S. A. Schaub, D. R. Alexander, and J. P. Barton, ''Theoretical model for the image formed by spherical particle in a coherent imaging system: comparison to experiment,'' *Opt. Eng.* **23**, 565–571 (1989).
8. B. Ovryn, T. Wright, and J. D. Khaydarov, ''Measurement of three-dimensional velocity profiles using forward scattering particle image velocimetry (FSPIV) and neural net pattern recognition,'' *Proc. SPIE* **2546**, 112–123 (1995).
9. Yuval Fisher, *Fractal Image Compression*, pp. 43–44, Springer Verlag, Berlin.
10. Z. Jinhui and Y. Yingbai, ''Global/local united search algorithm for global optimisation,'' *Optik (Stuttgart)* **4**, 161–164 (1998).
11. D. Goldberg, *Genetic Algorithms in Search, Optimization and Machine Learning*, Addison-Wesley, New York (1989).
12. Z. Michalewicz, *Genetic Algorithms+Data Structures=Evolution Programs*, 3rd ed., Springer-Verlag, Berlin.
13. C. R. Houck, J. Joines, and M. Kay, ''A genetic algorithm for function optimization: A Matlab implementation,'' in *ACM Transactions on Mathematical Software* (1996).
14. R. Menzel and F. M. Shofner, ''An investigation of Fraunhöfer holography for velocimetry applications,'' *Appl. Opt.* **9**, 2073–2079 (1970).
15. M. Funes-Gallanzi, ''A numerical investigation of flow past a bluff body using three-state anemometry (3SA),'' *Intl. J. Computational Methods in Fluids* **26**, 1023–1038 (1998).
16. J. E. Unruh and E. M. Mikhail, ''Mensuration tests using digital images,'' *Photogramm. Eng. Remote Sens.* **48**(8), 1343–1349 (1982).
17. H. Meng, ''Development of holographic particle image velocimetry,'' PhD dissertation, University of Houston, Texas (1994).
18. P. J. Bryanston-Cross, M. Funes-Gallanzi, C. Quan, and T. R. Judge, ''Holographic particle image velocimetry (HPIV),'' *Opt. Laser Technol.* **24**(5), 251–256 (1992)
19. C. Gray and C. A. Greated, ''A processing system for the analysis of particle displacement holograms,'' in *Optical Diagnosis in Fluid and Thermal Flow*, San Diego, CA, July 14–16, 1993.
20. H. Royer, ''Holographic particle image velocimetry,'' *Meas. Sci. Technol.* **8**, 1562–1572 (1997).
21. J. D. Trollinger, ''Development and application of holographic particle image velocimetry techniques for microgravity applications,'' *Meas. Sci. Technol.* **8**(12), 1573–1583 (1997).
22. D. D. Udrea, W. K. Lee, M. Burnett, P. Bryanston-Cross, and W. S. Cheung, ''Three-component particle tracking velocimetry by defocusing, in particle image velocimetry,'' in *Progress Towards Industrial Application*, M. Stanislas, J. Kompenhans, and J. Westerweel, Eds., pp. 479–494, Kluwer Academic Publisher, Norwell, MA (2000).
23. S. Murata and M. Kawamura, ''Particle depth measurement based on depth-from-defocus,'' *Opt. Laser Technol.* **31**, 95–102 (1999).